



**HAL**  
open science

## Periodic variations of oxygen EUV dayglow in the upper atmosphere of Venus: Hisaki/EXCEED observations

K. Masunaga, K. Seki, N. Terada, F. Tsuchiya, T. Kimura, K. Yoshioka, G. Murakami, A. Yamazaki, M. Kagitani, Chihiro Tao, et al.

### ► To cite this version:

K. Masunaga, K. Seki, N. Terada, F. Tsuchiya, T. Kimura, et al.. Periodic variations of oxygen EUV dayglow in the upper atmosphere of Venus: Hisaki/EXCEED observations. *Journal of Geophysical Research. Planets*, 2015, 120 (12), pp.2037-2052. 10.1002/2015JE004849 . insu-01240163

**HAL Id: insu-01240163**

**<https://insu.hal.science/insu-01240163>**

Submitted on 28 Aug 2020

**HAL** is a multi-disciplinary open access archive for the deposit and dissemination of scientific research documents, whether they are published or not. The documents may come from teaching and research institutions in France or abroad, or from public or private research centers.

L'archive ouverte pluridisciplinaire **HAL**, est destinée au dépôt et à la diffusion de documents scientifiques de niveau recherche, publiés ou non, émanant des établissements d'enseignement et de recherche français ou étrangers, des laboratoires publics ou privés.

## RESEARCH ARTICLE

10.1002/2015JE004849

## Key Points:

- Periodic variations of the EUV oxygen dayglow are observed at Venus
- The solar EUV flux controls main periodic variations of the oxygen dayglow
- Atmospheric waves and the solar wind may control minor dayglow periodicities

## Correspondence to:

K. Masunaga,  
masu-kei@stelab.nagoya-u.ac.jp

## Citation:

Masunaga, K., et al. (2015), Periodic variations of oxygen EUV dayglow in the upper atmosphere of Venus: Hisaki/EXCEED observations, *J. Geophys. Res. Planets*, 120, 2037–2052, doi:10.1002/2015JE004849.

Received 7 MAY 2015

Accepted 25 OCT 2015

Accepted article online 28 OCT 2015

Published online 2 DEC 2015

## Periodic variations of oxygen EUV dayglow in the upper atmosphere of Venus: Hisaki/EXCEED observations

K. Masunaga<sup>1,2</sup>, K. Seki<sup>1,2</sup>, N. Terada<sup>3</sup>, F. Tsuchiya<sup>4</sup>, T. Kimura<sup>5</sup>, K. Yoshioka<sup>2,6</sup>, G. Murakami<sup>7</sup>, A. Yamazaki<sup>7</sup>, M. Kagitani<sup>4</sup>, C. Tao<sup>8,9</sup>, A. Fedorov<sup>8</sup>, Y. Futaana<sup>10</sup>, T. L. Zhang<sup>11</sup>, D. Shiota<sup>1</sup>, F. Leblanc<sup>12</sup>, J.-Y. Chaufray<sup>12</sup>, and I. Yoshikawa<sup>13</sup>

<sup>1</sup>Institute for Space-Earth Environmental Research, Nagoya University, Nagoya, Japan, <sup>2</sup>Department of Earth and Planetary Science, Graduate School of Science, University of Tokyo, Tokyo, Japan, <sup>3</sup>Department of Geophysics, Graduate School of Science, Tohoku University, Sendai, Japan, <sup>4</sup>Planetary Plasma and Atmospheric Research Center, Graduate School of Science, Tohoku University, Sendai, Japan, <sup>5</sup>Nishina Center for Accelerator Based Science, RIKEN, Wako, Japan, <sup>6</sup>Department of Physics, Rikkyo University, Tokyo, Japan, <sup>7</sup>Institute of Space and Astronautical Science, Japan Aerospace Exploration Agency, Sagami-hara, Japan, <sup>8</sup>IRAP, Université de Toulouse/UPS-OMP/CNRS, Toulouse, France, <sup>9</sup>National Institute of Information and Communications Technology, Tokyo, Japan, <sup>10</sup>Swedish Institute of Space Physics, Kiruna, Sweden, <sup>11</sup>Space Research Institute, Austrian Academy of Sciences, Graz, Austria, <sup>12</sup>LATMOS, Guyancourt, France, <sup>13</sup>Department of Complexity Science and Engineering, University of Tokyo, Kashiwa, Japan

**Abstract** Using the Extreme Ultraviolet Spectroscope for Exospheric Dynamics (EXCEED) aboard Hisaki and the Solar Extreme Ultraviolet Monitor on the Solar and Heliospheric Observatory, we investigate variations of the extreme ultraviolet (EUV) dayglow brightness for OII 83.4 nm, OI 130.4 nm, and OI 135.6 nm in the Venusian upper atmosphere observed in March–April (period 1), April–May (period 2), and June–July (period 3) in 2014. The result shows that characteristic periodicities exist in the dayglow variations other than the ~27 day solar rotational effect of the solar EUV flux: 1.8, 2.8, 3.1, 4.5, and 9.9 day in period 1; 1.1 day in period 2; and 1.0 and 11 day in period 3. Many of these periodicities are consistent with previous observations and theory. We suggest these periodicities are related to density oscillations of oxygen atoms or photoelectrons in the thermosphere. The cause of these periodicities is still uncertain, but planetary-scale waves and/or gravity waves propagating from the middle atmosphere, and/or minor periodic variations of the solar EUV radiation flux may play a role. Effects of the solar wind parameters (velocity, dynamic pressure, and interplanetary magnetic field's intensity) on the dayglow variations are also investigated using the Analyser of Space Plasma and Energetic Atoms (ASPERA-4) and magnetometer aboard Venus Express. Although clear correlation with the dayglow variations is not found, their minor periodicities are similar to the dayglow periodicities. Contribution of the solar wind to the dayglow remains still unknown, but the solar wind parameters might affect the dayglow variations.

### 1. Introduction

In the Venus thermosphere, there is a temperature difference between the day and night due to a solar heating. This makes a large horizontal pressure gradient in the Venus thermosphere. Thus, the subsolar to antisolar (SS-AS) flow becomes a dominant flow pattern above 120 km altitudes although the atmosphere is zonally rotating westward below 70 km altitudes [e.g., Bougher *et al.*, 1997]. At ~100 km altitudes in the mesosphere, the zonal wind speed is observed to be highly variable [Lellouch *et al.*, 1997].

The westward zonal wind speed becomes strongest, on the order of ~100 m/s in the thick cloud at 70 km altitude, which is called the superrotation. Although mechanisms to drive and maintain the superrotation is yet to be known, past studies have shown that atmospheric waves, such as the Kelvin waves, the Rossby waves, and thermal tides, could play an important role for the formation and maintenance of the superrotation [e.g., Del Genio and Rossow, 1990; Takagi and Matsuda, 2007]. These waves zonally propagate with a periodicity of 4 day for the Kelvin waves and of 5.6 day for the Rossby waves and of 117 day for thermal tides [Del Genio and Rossow, 1990; Yamamoto and Tanaka, 1997; Takagi and Matsuda, 2007].

Recently, Forbes and Konopliv [2007] reported that periodic density variations exist in the Venus thermosphere at 164–184 km altitudes. In the density variations, they found a 9 day periodicity in the nightside and a 10 day periodicity in the dayside, respectively. They also found a 4.7 day periodicity in the dayside

thermosphere although data was not shown because they focused on the 9 day periodicity observed in the nightside thermosphere. It was suggested that these density variations resulted from the planetary-scale waves propagating from the middle atmosphere of Venus and were caused by wave-wave interactions between planetary-scale waves with 2.8 day periodicity and those with 4 day periodicity.

More recently, it is reported that the Kelvin waves and the Rossby waves imposed in the middle atmosphere (at 80 km altitudes) can propagate into the thermosphere (at 130 km altitudes) by using the general circulation model (GCM) [Hoshino *et al.*, 2012]. They showed that the Kelvin waves affect the general circulation in the thermosphere because the Kelvin waves propagate with large amplitudes.

Kouyama *et al.* [2015] showed that characteristics of the vertical propagation of the Kelvin waves and the Rossby waves from the lower atmosphere (60 km altitudes) to the cloud top level (80 km altitudes) at Venus depend on background wind velocity. Under high background winds, the Kelvin waves reached to the cloud top, but the Rossby waves did not. In contrast, the Rossby waves reached to the cloud top but the Kelvin waves did not under the slow background wind.

Nakagawa *et al.* [2013] showed that there are modulations of the SS-AS flow velocity at 110 km altitudes of Venus by observing Doppler wind velocities of the infrared CO<sub>2</sub> emission at 10.5  $\mu\text{m}$  from the ground-based observatory and that the wind modulations are larger than those caused by the Kelvin waves calculated by the GCM used in Hoshino *et al.* [2012]. They suggested that gravity waves originating from the middle atmosphere are a possible source to cause the large wind modulations in the thermosphere.

The effect of gravity waves on the Venus thermospheric circulation is studied in Alexander [1992]. She suggested that gravity waves propagate from the Venus cloud level or just above into the thermosphere, resulting in wave-induced accelerations of the thermospheric superrotation. The gravity waves generate enhanced eddy diffusions in the Venus thermosphere. Alexander *et al.* [1993] reported a significant dawn-dusk asymmetry in the brightness of the oxygen dayglow emission at 130.4 nm by using the Ultraviolet Spectrometer aboard Pioneer Venus Orbiter. Using their Venus thermosphere general circulation model, they showed that the SS-AS flow pattern coupled to a steady supply of gravity waves from the middle atmosphere provides asymmetric eddy diffusions and explains the observed dawn-dusk asymmetry.

The Venus upper atmosphere may also be affected by the solar wind due to the absence of an intrinsic magnetic field at Venus. The solar wind can reach down to the top of the ionosphere (typically,  $\sim 300$  km at the subsolar region and  $\sim 900$  km near the terminator [Phillips *et al.*, 1985]) and the interplanetary magnetic field (IMF) piles up on the ionosphere. This results in producing the induced magnetosphere at Venus. The solar wind dynamic pressure is balanced at the induced magnetosphere boundary (IMB), thus the IMB altitude depends on the solar wind [Zhang *et al.*, 1991]. The altitude of the upper boundary of the ionosphere (ionopause) also changes depending on the solar wind's dynamic pressure [Russell and Vaisberg, 1983].

Lei *et al.* [2008] found 9 day periodicities in density variations in the thermosphere of the Earth. They suggested that the 9 day modulations can be caused by three groups of solar coronal holes located equidistantly around the Sun, which leads to temporal arrivals of the coronal interaction regions (CIR) and geometric disturbances at Earth. They further mentioned that the 9 day density modulations at the Venus thermosphere shown in Forbes and Konopliv [2007] could be caused by the solar wind dynamic pressure's modulations.

According to the studies shown above, the Venus upper atmosphere could be affected both by the atmospheric waves propagating from the middle atmosphere and by the solar wind. However, a relationship between the Venus upper atmosphere, middle atmosphere, and the solar wind is still uncertain. To give understandings of their relationship, we investigate variations of the EUV dayglow in the upper atmosphere of Venus by using the EUV spectroscopy on the Earth orbiting spacecraft, Hisaki. Unlike Venus orbiters, Hisaki can always collect all EUV photons coming from the Venus disk from the Earth orbit although the spatial resolution is poor compared to Venus orbiter's observations. Thus, Hisaki is a useful tool to see global changes of the various dayglow emissions, namely, global density changes of various components in the Venus upper atmosphere. We focus on the major oxygen dayglow emission lines for OII 83.4 nm, OI 130.4 nm, and OI 135.6 nm seen in the Venus thermosphere [Moos and Rottman, 1971; Broadfoot *et al.*, 1974; Stewart *et al.*, 1979; Bertaux *et al.*, 1981; Hord *et al.*, 1991; Feldman *et al.*, 2000; Hubert *et al.*, 2010; Gérard *et al.*, 2011]. The OII 83.4 nm emission is excited by the photoelectron impacts on O atoms and by the solar resonant scattering on O<sup>+</sup> ions. The contribution of the resonant scattering to the intensity is very small ( $\sim 0.3\%$ ) thus can be

neglected [Gérard *et al.*, 2011]. The 130.4 nm emission is excited by the photoelectron impacts and the solar resonant scattering on O atoms. The photoelectron impacts are the dominant source in the lower thermosphere (<180 km) but the resonant scattering becomes the dominant source in the higher thermosphere [Alexander *et al.*, 1993]. The 130.4 nm emission is optically thick so that its brightness does not always provide a content of O atoms in the Venusian thermosphere. In contrast, the 135.6 nm emission is mainly excited by photoelectron impacts on O atoms and its emission is optically thin. Thus, its brightness is proportional to the content of O atoms and the content of the photoelectrons in the thermosphere.

In this study, we study the variations of the EUV dayglow in terms of periodicities that correspond to those of atmospheric waves in the middle atmosphere observed in previous studies to see relations between the upper atmosphere and the middle atmosphere of Venus. The dependence of the EUV dayglow variations on the solar EUV radiation flux observed by the Solar and Heliospheric Observatory is also studied since the amount of photoelectrons in the Venus ionosphere is controlled by the solar helium line (30.4 nm) [Spenner *et al.*, 1997; Coates *et al.*, 2008] and affects the EUV dayglow excited by the photoelectron impacts. We also study effects of the solar wind parameters such as the velocity, dynamic pressure, and the intensity of the interplanetary magnetic field (IMF) on the oxygen dayglow variations by using plasma and field measurements observed by Venus Express and discuss how the solar wind is connected to the photoelectron content and the thermosphere of Venus.

## 2. Instrumentations and Data Processing

### 2.1. Instrumentations

We use four instruments in this study: the Extreme Ultraviolet Spectroscope for Exospheric Dynamics (EXCEED) [Yoshioka *et al.*, 2013; Yoshikawa *et al.*, 2014] aboard Hisaki, the Solar Extreme Ultraviolet Monitor (SEM) [Hovestadt *et al.*, 1995] on the Solar and Heliospheric Observatory (SOHO), and the Analyser of Space Plasma and Energetic Atoms (ASPERA-4) [Barabash *et al.*, 2007] and the magnetometer (MAG) [Zhang *et al.*, 2006] aboard Venus Express (VEX). Hisaki is a small satellite of the mission of the Small scientific satellite Platform for Rapid Investigation and Test-A, which was launched on 14 September 2013 into the orbit around the Earth with an altitude of ~1000 km and an inclination of ~30°. Hisaki carries the EXCEED instrument to observe EUV emissions from planetary plasma and atmosphere such as Venus, Mars, and Jupiter. In 2014, Hisaki observed EUV dayglow of Venus during the three quasi-continuous periods: 9 March to 2 April (period 1), 24 April to 23 May (period 2), and 24 June to 17 July (period 3). EXCEED has three different slits whose width is 10", 60" and 140" and uses one of them depending on a target planet. The 60" slit is used when observing Venus. The field of view guiding camera allows to track the target planet and to fix it in the slit [Yamazaki *et al.*, 2014]. The pointing accuracy depends on observational modes. For observations using the 60" slit, "Hold mode" is applied and the pointing accuracy is 20–25". EXCEED counts photons with 1 s resolution. In this study we use 1 min accumulated spectrum (level 2 data). For the level 2 data, photons measured by EXCEED are converted into the spatial-spectral image (1024 pixels × 1024 pixels). Observable range of the wavelength is 52–148 nm with a resolution of ~0.8 nm [Yoshioka *et al.*, 2013]. The field of view of the slit is 360°. Pixel sizes of the level 2 data are ~4.2" in the spatial direction and ~10" in the spectral direction.

The Solar Extreme Ultraviolet Monitor (SEM) is one of the instruments on the Solar and Heliospheric Observatory (SOHO) [Domingo *et al.*, 1995]. A detailed description of SEM is shown in Hovestadt *et al.* [1995]. SEM has been observing nearly continuous solar EUV irradiance since December 1995, and it provides the solar radiation flux in two bands: 26–34 nm and 0.1–50 nm. We use the former solar radiation flux as a proxy for the amount of photoelectrons in the Venus ionosphere because the helium 30.4 nm line controls the amount of photoelectrons in the Venus ionosphere [Spenner *et al.*, 1997; Coates *et al.*, 2008]. Since our interest is the EUV flux at Venus, the data period of SEM is shifted by several days depending on the angle between the Sun-Earth line and the Sun-Venus line by assuming the 27 day solar rotation. The angle changes from 35° to 50° in period 1, from 62° to 80° in period 2, and from 100° to 115° in period 3.

ASPERA-4 comprises two plasma sensors and two sensors for energetic neutral atoms. We use the two plasma instruments in this study: Ion mass Analyzer (IMA) and Electron Spectrometer (ELS). IMA observes ions with mass separations. The energy range of IMA is 0.01–40 keV with an energy resolution of 7%. The field of view is 360° × 90° with 16 × 16 sectors giving a resolution of 22.5° × 5.6°. Ion moments are obtained from full 3-D ion velocity distribution functions, and its time resolution is 192 s. A part of the ion velocity distribution function is often obscured by the spacecraft body, by spacecraft parts such as solar arrays, and by the limited field of view of IMA.

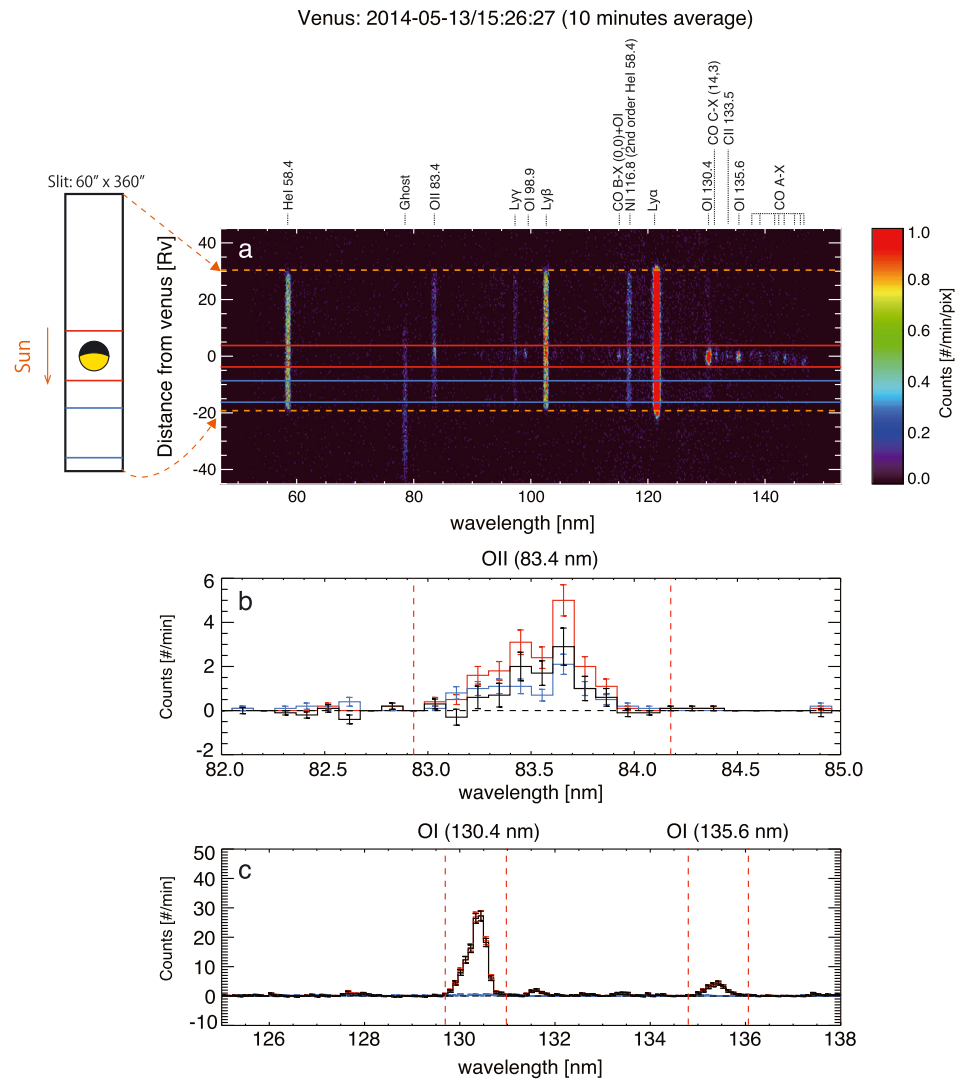


**Figure 1.** (a) 10 min average spectrum of Venus observed on 13 May 2014. Slit is aligned with the Venus-Sun line as shown in the left illustration. Horizontal axis indicates wavelength, vertical axis shows distance from Venus, and color codes display count rates. The ghost at ~78 nm is caused by the Lyman alpha reflected by the detector surface and grating in the EXCEED instrument [Yoshikawa *et al.*, 2014]. Horizontal red and blue lines in the image indicate spatial ranges in which counts are integrated to make spectra of the disk and the sky, respectively. (b, c) Integrated spectra of the Venus disk (red), the geocorona (blue), and the dayglow emission (black) for OII 83.4 nm, OI 130.4 nm, and OI 135.6 nm. Vertical red dashed lines indicate a spectral range to integrate counts in order to obtain the dayglow intensity of the Venus disk for each emission line.

The quality index of the ion moment data, ranging from 0 to 1, indicates a degree of the nonobscured part of the ion velocity distribution function. For better accuracy, we only use the ion moment data with the quality index > 0.95. We use IMA as a solar wind proton monitor, so we only use the proton moment in the period when VEX flies in the solar wind. ELS observes electrons with an energy of 0.01–20 keV with an energy resolution of 7%. The field of view is 360° × 4° with an azimuth plane divided into 16 sectors giving each 22.5° wide. We use ELS data to define an altitude of the induced magnetosphere boundary and to see how the size of the induced magnetosphere changes depending on the change of the solar wind’s dynamic pressure. Note that VEX orbits around Venus every ~24 h and ASPERA-4 is usually operated for several hours only around the peri-center and the apocenter.

The magnetometer (MAG) is composed of two triaxial fluxgate sensors and measures the magnetic field vector. The detail design of MAG is described in Zhang *et al.* [2006]. In this study we use minutely averaged

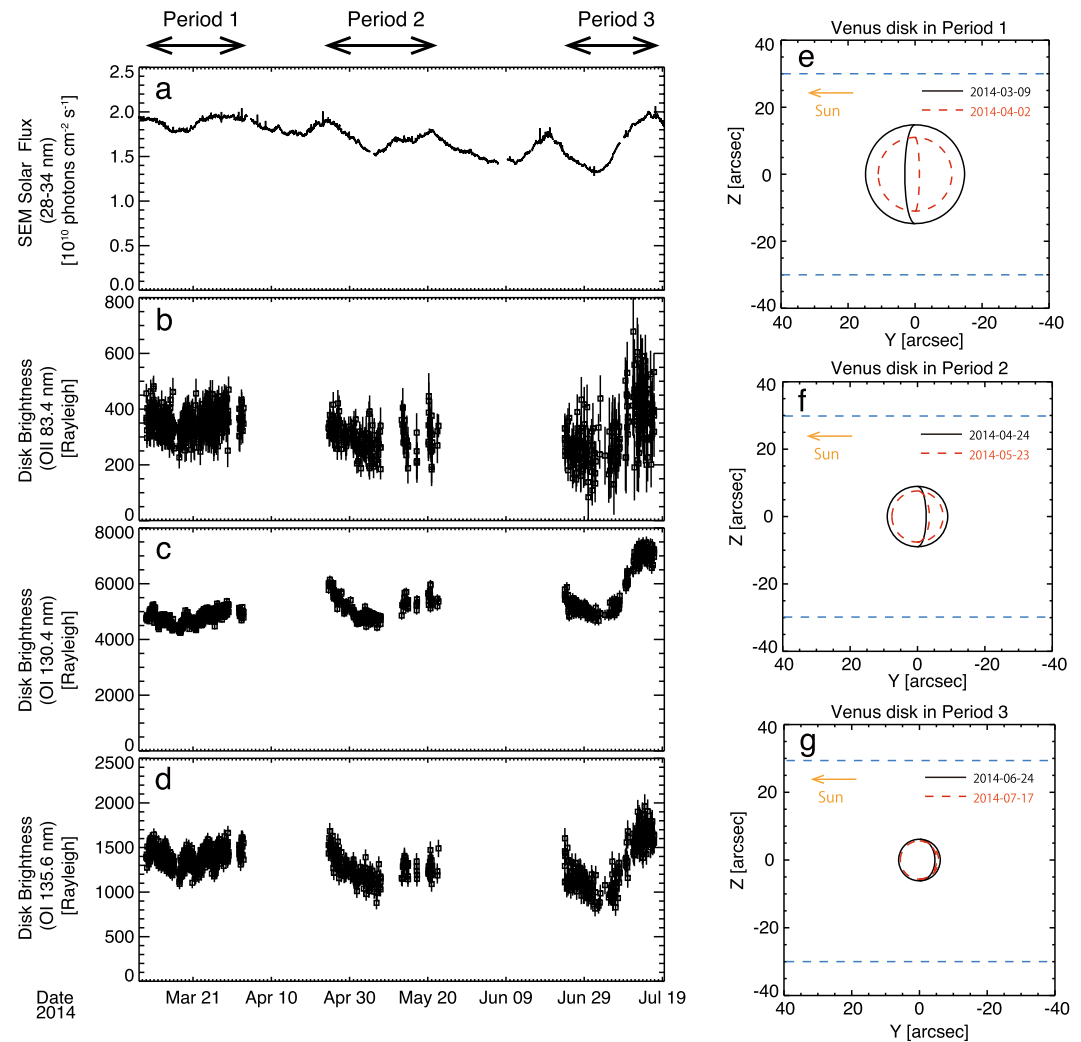


**Figure 2.** Time series of the (a) 10 min average solar EUV radiation flux for 28–34 nm shifted to Venus and brightness of the EUV dayglow for (b) OII 83.4 nm, (c) OI 130.4 nm, (d) OI 135.6 nm. Venus disk viewed from the Earth in (e) period 1, (f) period 2, and (g) period 3. The line of sight from the Earth is the X axis (perpendicular to the plane). The Y axis is set to be parallel to a perpendicular component of the Venus-Sun line to the line of sight, and the Z axis completes the right-hand system. The black line indicates the Venus disk on the beginning of each period, and the red dashed line indicates the Venus disk in the end of each period. Blue dashed lines are edges of the slit.

data set of MAG. As for the ASPERA-4 data, we only use the data in the period that VEX is in the solar wind so the measurements correspond to the interplanetary magnetic field (IMF).

**2.2. Processing of EXCEED Data**

Figure 1a shows a sample EUV spectrum observed by EXCEED in period 2. For better statistics, we have integrated 10 spectra (10 min) and made an average spectrum. As shown by the illustration on the left side of Figure 1a, the slit of EXCEED is aligned with the Venus-Sun line. Note that Venus was not slit filling in any of the observation periods as similar as this illustration (see also appearances of the Venus disk in the slit in each period shown in Figures 2e–2g). The Venus disk is placed 100" (period 1) or 50" sunward (periods 2 and 3) from the center of the slit because we are also interested in estimating escaping ions in the Venus tail for another study. In this spectrum many dayglow emissions are identified around Venus as seen in previous studies [Feldman et al., 2000; Gérard et al., 2011]. However, some of them include geocoronal emissions spreading out in the slit. In this study we focus on the major oxygen dayglow for OII 83.4 nm, OI 130.4 nm, and OI 135.6 nm. In order to obtain emissions of this dayglow, we need to remove the effect of the geocoronal emission for OII 83.4 nm and OI 130.4 nm.

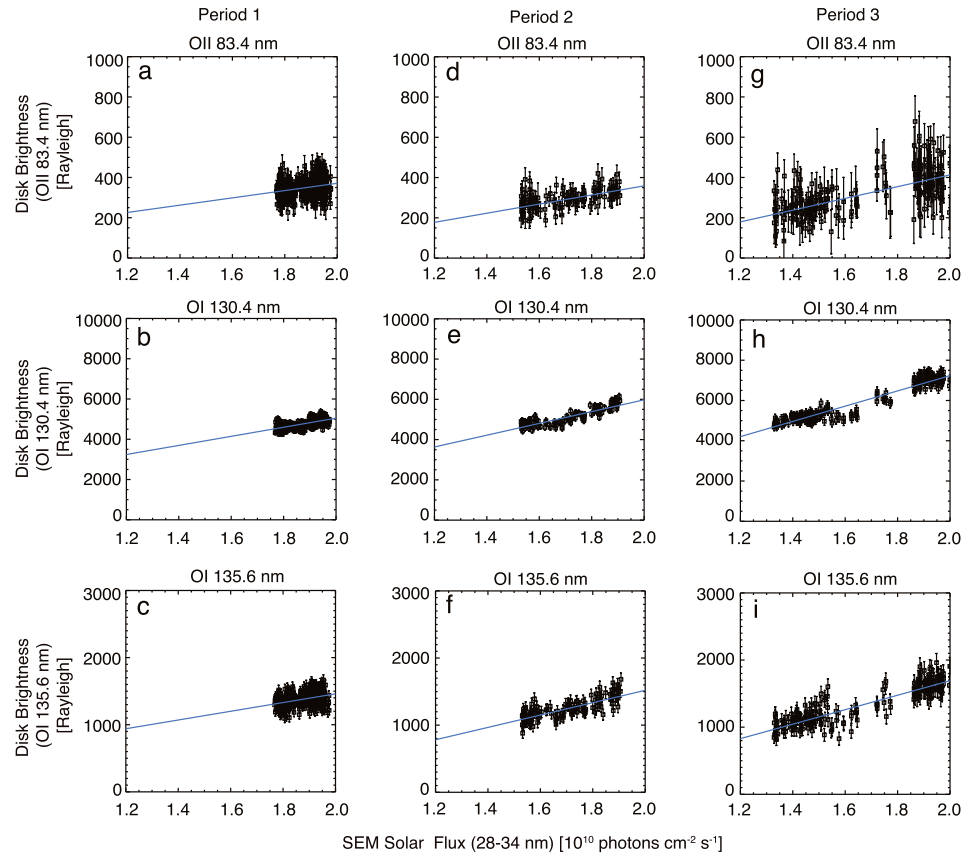


**Figure 3.** Scatterplots of the dayglow brightness and the solar EUV radiation flux for (a) OII 83.4 nm, (b) OI 130.4 nm, and (c) OI 135.6 nm for period 1. (d–i) The same plots for periods 2 and 3 are shown. A blue line in each panel indicates a linear fit for the relation between the solar flux and the dayglow brightness.

Figures 1b and 1c show spectra of these oxygen emissions. The red curves are total counts integrated within a region around the Venus disk (horizontal red lines in Figure 1a). The blue curves (horizontal blue lines in Figure 1a) are total counts integrated within a nearby region in the same exposure which does not contain Venus (typically  $> 10 R_V$  downstream from Venus for period 1,  $> 5 R_V$  upstream from Venus for periods 2, and  $> 8 R_V$  upstream from Venus for period 3), which are assumed to proxy the geocoronal emissions. By subtracting the geocoronal spectrum from the disk spectrum, we obtained the dayglow spectrum as shown by the black curves. We then integrate all counts of the broadening emission line in the range shown by vertical red dashed lines. Multiplying the calibrated geometric factor with the total counts of the dayglow emissions, we get absolute intensity of the dayglow emission. Note that count rates temporally change due to the change of the apparent diameter and the illuminating area of Venus over the three periods (see Figures 2e–2g). When calculating the absolute intensity, we correct these effects as observed at 1 AU from Venus with 100% illuminating area:

$$I = \frac{C \cdot f}{\pi(d/2)^2 (L_X \cdot L_Y)^{-1}} \times \frac{100}{A_i} \quad (1)$$

where  $I$  is the intensity (Rayleigh) and  $C$ ,  $d$ ,  $L_X$ ,  $L_Y$ ,  $A_i$ , and  $f$  are the count rates integrated from the apparent disk (count/min), the apparent diameter of Venus (arcsec), plate scales of the single pixel for the spectral (10") and spatial (4.2") directions, the illuminating area of Venus (%), and the geometric factor (Rayleigh(count/min) $^{-1}$  pix $^{-1}$ ), respectively. Adopting this method for each spectrum, we obtain time series of the oxygen dayglow emissions.

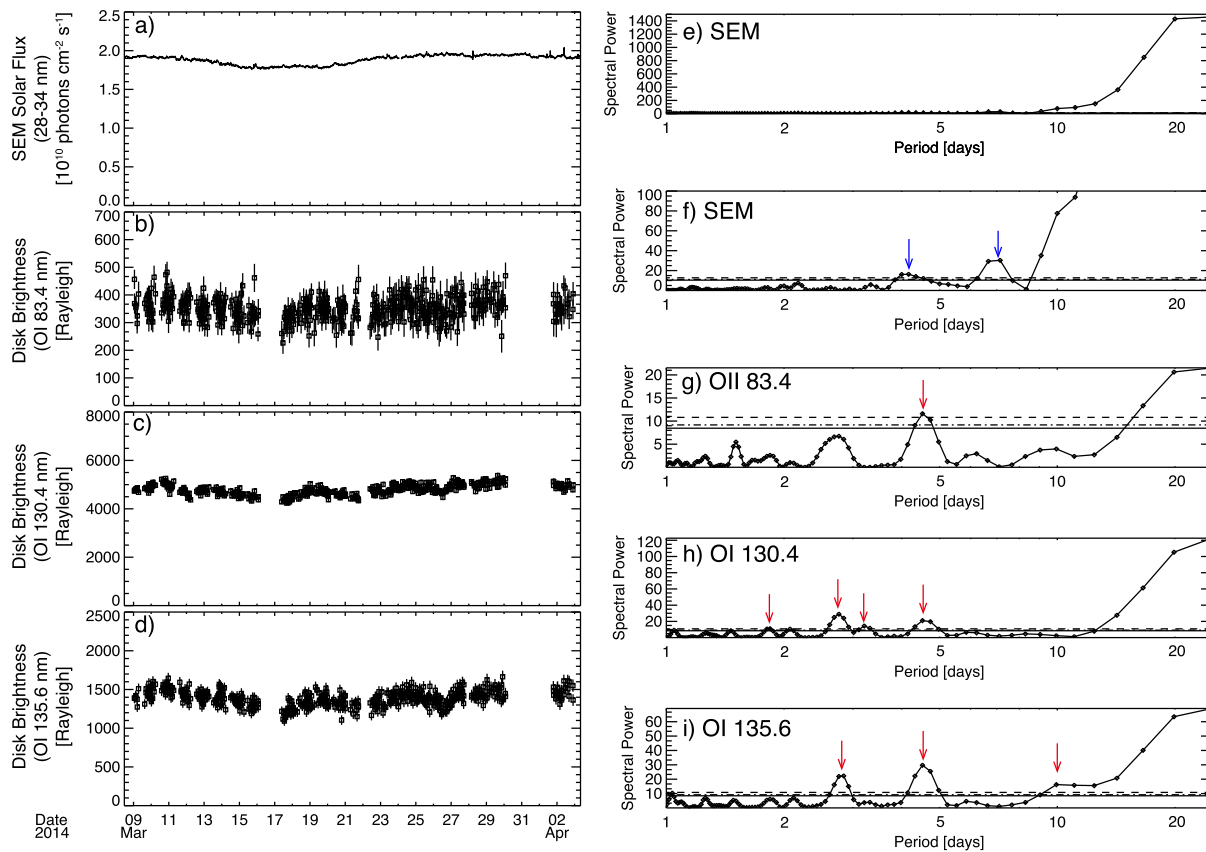


**Figure 4.** Time series of (a) the solar EUV radiation flux and the dayglow brightness for (b) OII 83.4 nm, (c) OI 130.4 nm, and (d) OI 135.6 nm for period 1. Normalized power spectrum for (e and f) the solar radiation flux and the dayglow brightness for (g) OII 83.4 nm, (h) OI 130.4 nm, and (i) 135.6 nm calculated by the Lomb-Scargle periodogram. Horizontal solid line, dashed dot line, and dashed lines indicate 90%, 95%, and 99% confidence levels, respectively. The blue and red arrows indicate peaks of characteristic periodicities exceeding the 99% confidence level.

### 3. Observations

#### 3.1. Characteristics of Oxygen Dayglow Variations

Figures 2a–2d show a time series of the 10 min average solar radiation flux for 28–34 nm observed by SEM and the dayglow brightness variation of OII 83.4 nm, OI 130.4 nm, and OI 135.6 nm. Average brightness over the three periods is 0.33 kR for OII 83.4 nm, 5.1 kR for OI 130.4 nm, and 1.3 kR for OI 135.6 nm, respectively. These intensities are nearly consistent with past observations [Alexander *et al.*, 1993; Feldman *et al.*, 2000; Hubert *et al.*, 2010]. Over the period, the solar radiation flux periodically varies due to the solar rotational effect (~27 days). We can see that the three dayglow emissions also vary similarly to the variations of the solar radiation flux. Figure 3 shows the correlation between the oxygen dayglow brightness (for three different wavelengths) and the solar radiation flux for three periods. All show positive correlations. Since these oxygen emissions are mainly excited by photoelectron impacts on O atoms, the solar radiation flux of the helium line (30.4 nm), which produces photoelectrons due to photoionizations of CO<sub>2</sub> molecules and O atoms in the Venusian ionosphere, controls the dayglow emissions. We further investigate a difference from these relations. We fitted each emission's brightness by the solar flux using a linear regression (blue lines in each panel in Figure 3). The residual brightness with respect to the fitted intensity, in principle, does not contain the dependence on the solar rotational effect. The 1 sigma variations of the residual brightness with respect to the fitted intensity are 12% for OII 83.4 nm, 3.4% for OI 130.4 nm, and 6.6% for OI 135.6 nm in period 1; 14% for OII 83.4 nm, 4.0% for OI 130.4 nm, and 7.8% for OI 135.6 nm in period 2; and 27% for OII 83.4 nm, 4.7% for OI 130.4 nm, and 10% for OI 135.6 nm in period 3. We assume that these variations come from different effects from the solar rotational effect (~27 days).

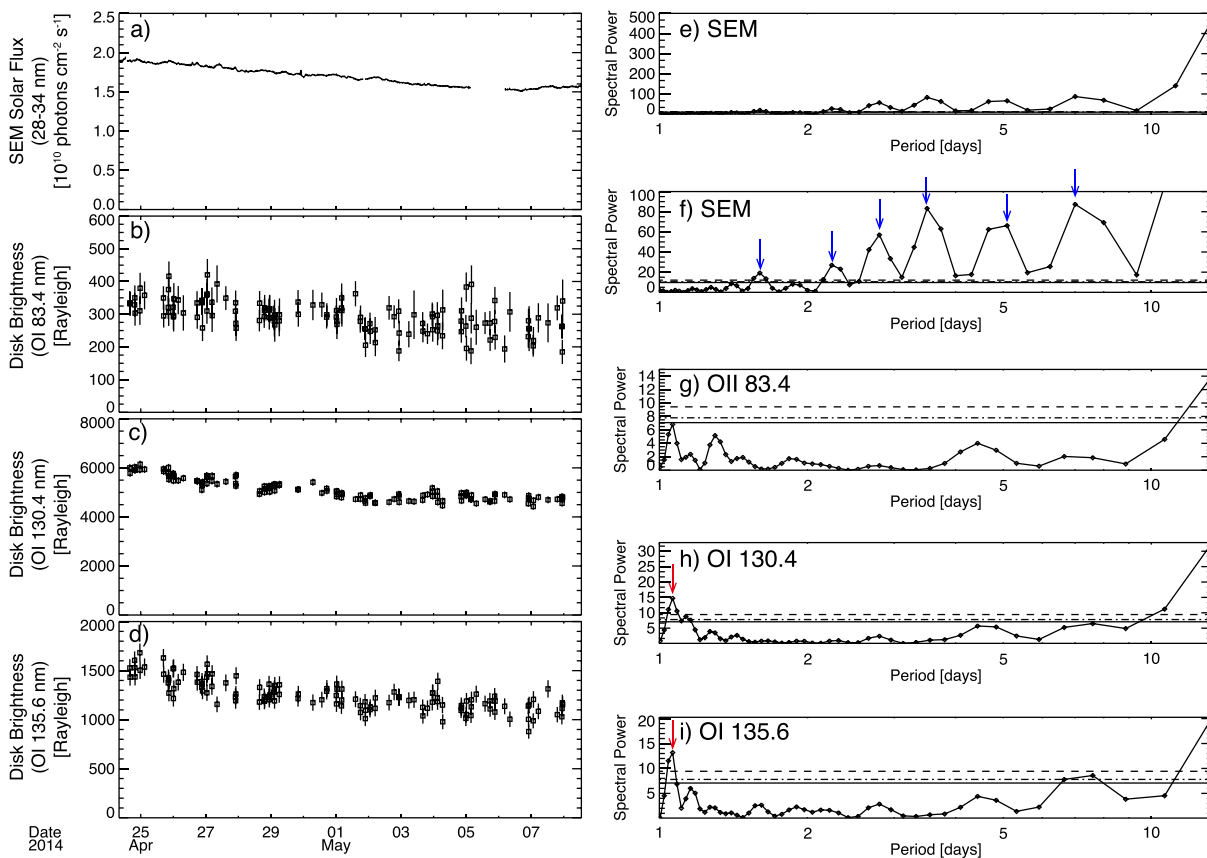


**Figure 5.** Time series of the solar EUV radiation flux and the dayglow brightness and the normalized power spectra for period 2. The format is the same as Figure 4. Note that we show data period between 24 April and 7 May because there are large data gaps after 8 May.

Figures 4a–4d show time series of the solar radiation flux and dayglow variations for period 1. During this period, each variation looks similar and seems to have certain periodicities other than the solar rotational effect (~27 days). Figures 4e–4i show normalized power spectra for the variation of the solar radiation flux and the dayglow brightness calculated by using the Lomb-Scargle periodogram (LSP) method [Lomb, 1976; Scargle, 1982]. This method allows us to calculate a power spectrum for unevenly sampled data. In this power spectrum, we set the range of the period (the horizontal axis) from 1 day, which is much larger than the Nyquist period of each data, to the period of the data span. In Figure 4e, we can see that most of the power concentrate in the period of > 20 days even though we do not identify the peak. This power likely comes from the solar rotational effect. Figure 4f is the same as the Figure 4e but the range of the power is limited to see small power peaks. We identify two peaks exceeding the 99% significant level (a horizontal dashed line in the spectrum) at ~4.3 day and ~7.1 day as indicated by blue arrows. On one hand, the three dayglow emissions show similar spectra as seen in Figures 4g–4i. The strongest power > 20 days out of the data span is due to the solar rotational effect. However, we see a clear peak at ~4.5 day above the 99% confidence level for all emission lines. A period of ~2.8 day is also observed for OI 130.4 nm OI 135.6 nm. We also see small peaks of ~1.8 day and ~3.1 day for OI 130.4 nm and an unclear peak of ~9.9 day for OI 135.6 nm, respectively.

Figure 5 shows a time series of the solar radiation flux and the dayglow variations for period 2, and their power spectra calculated by the LSP method. The format is the same as Figure 4. Note that we only used data period between 24 April and 7 May since there are large data gaps in the dayglow data after 7 May (see Figures 2b–2d). We can see that variations of the dayglow brightness look similar to the variation of the solar radiation flux and seem to have certain periodicities (Figures 5a–5d). As seen in Figure 5e, the power of the solar radiation flux mostly concentrates at periodicities out of the data span. This is likely to be caused by the ~27 day periodicity of the solar rotational effect. In Figure 5f, we identify several periodicities above the 99% confidence level in the solar radiation flux as indicated by blue arrows: ~1.6 day, ~2.2 day, ~2.8 day,

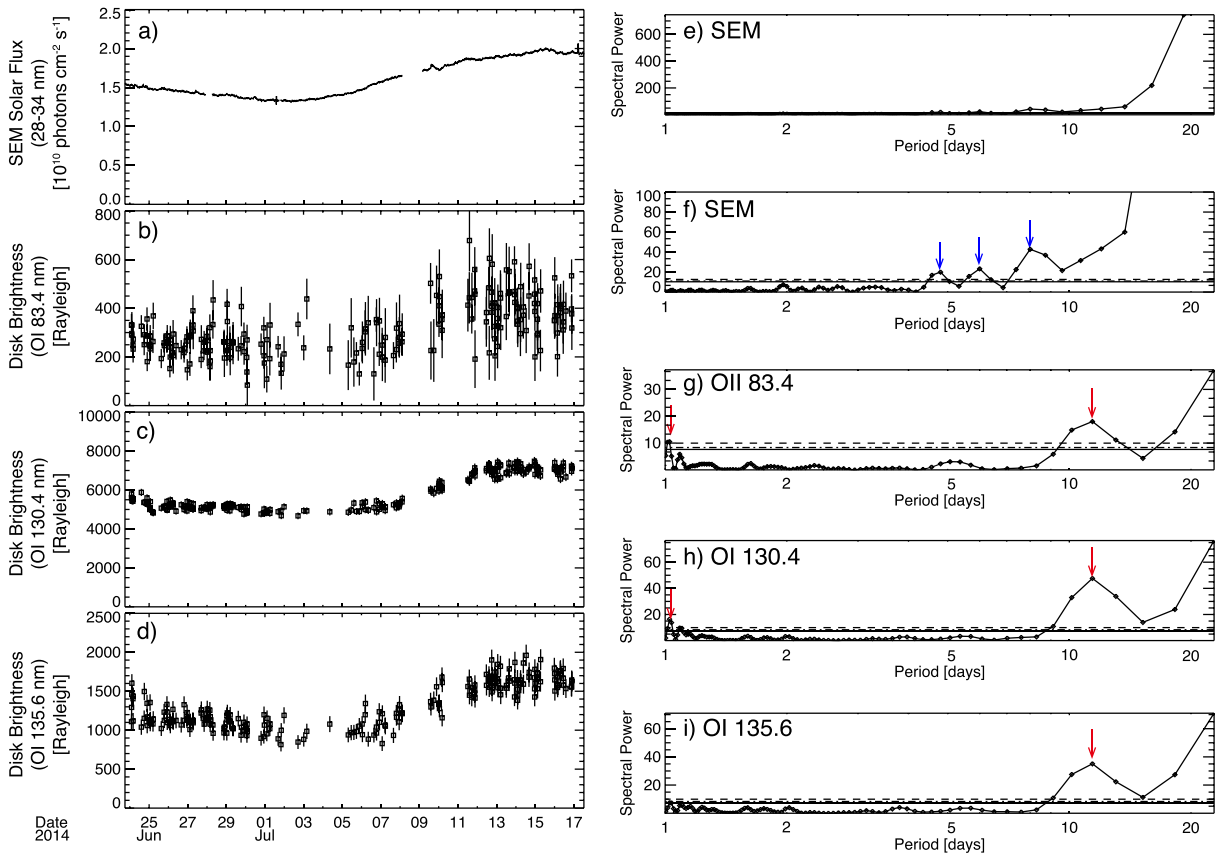


**Figure 6.** Time series of the solar EUV radiation flux and the dayglow brightness and the normalized power spectra for period 3. The format is the same as Figure 4.

~3.5 day, ~5.1 day, and 7.0 day. On one hand, the power spectrum of the three dayglow emissions look similar as seen in Figures 5g–5i. As indicated by red arrows, we only identify a periodicity of ~1.1 day above the 99% confidence level for OI 130.4 nm and OI 135.6 nm in this period.

Figure 6 shows the time series of the solar flux and the oxygen dayglow brightness for period 3, and their power spectra calculated by the LSP method. The format is the same as Figures 4 and 5. As seen in Figures 6a–6d, all dayglow emissions look to vary similarly to the variation of the solar flux although there are large errors in OII 83.4 nm. The solar radiation flux shows the strongest power at > 20 days due to the solar rotational effect (Figure 6e). In addition to this, three peaks in periodicities above the 99% confidence level are identified at ~4.8 day, ~6.0 day, and ~8.0 day as indicated by blue arrows in Figure 6f. On one hand, in Figures 6g–6i, we can see a periodicity at ~11 day for all the three emissions, and at ~1.0 day for OII 83.4 nm (Figure 6g) and OI 130.4 nm (Figure 6h).

### 3.2. Simultaneous Observation of the Solar Wind

In this subsection, we study simultaneous observation of the solar wind parameters with the variations of the brightness of the oxygen dayglow. First, we investigate relationship between the dayglow variations and sudden changes of the solar wind parameters. Figures 7a–7i show the time series of the absolute disk brightness ((a) OII 83.4 nm, (b) OI 130.4 nm, and (c) OI 135.6 nm), the solar wind parameters ((d) proton bulk speed, (e) proton number density, (f) dynamic pressure, and (g) magnetic field intensity) observed by IMA and MAG, (h) the altitude of the induced magnetosphere boundary (IMB) observed by ELS, and (i) the solar zenith angle of the location when VEX crosses the IMB. The solar wind parameters are observed when VEX is outside the bow shock, namely, in the solar wind region. Note that ASPERA-4 is usually operated only near the periapsis and the apoapsis while MAG works almost all the time. Thus, the two instruments have different periods of data sampling. Unfortunately, magnetic field data are mostly lacking in period 1 as seen in Figure 7g. During period 1, VEX observes two corotational interaction regions (CIRs) and six enhancements of the dynamic pressure as

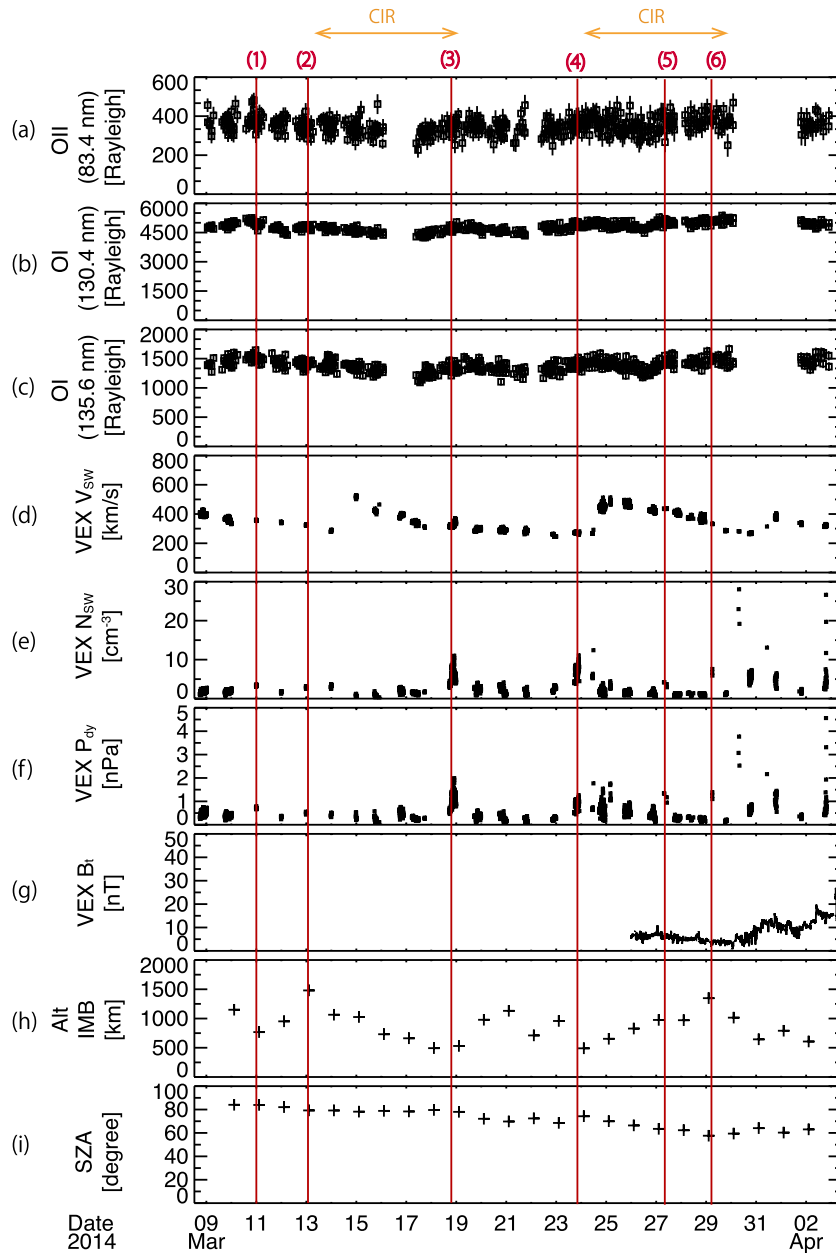


**Figure 7.** Time series of dayglow brightness for (a) OII 83.4 nm, (b) OI 130.4 nm, and (c) OI 135.6 nm; (d) proton speed, (e) proton number density, (f) dynamic pressure of the solar wind observed by IMA, and (g) IMF intensity observed by MAG; (h) the altitude of the induced magnetosphere boundary (IMB) determined by ELS; and (i) the solar zenith angle when VEX crosses the IMB in period 1. Red vertical lines indicate times when VEX observed solar wind dynamic pressure enhancements.

shown by orange arrows and red numbered vertical lines in the time series panels of Figure 7. When high dynamic pressure reaches to Venus, we can mostly see that the IMB altitude is starting to decrease, is decreasing or is prevented from recovering (see high-pressure events 1, 2, and 4–6). Despite the large changes of the IMB altitude, we do not find common features in the dayglow variations at the high-pressure events.

Figures 8 shows the time series of the disk brightness, solar wind parameters, the IMB altitude, and the solar zenith angle of the VEX position observed in period 2. The format is the same as Figure 7. As seen in Figures 8d and 8e, the solar wind parameters look relatively stable compared with that of period 1. We only see enhancements of the solar wind dynamic pressure and the IMF intensity on 3 May (a red vertical line) and 6 May (a blue vertical line), respectively, and there is no common feature coincidentally seen with the brightness variations.

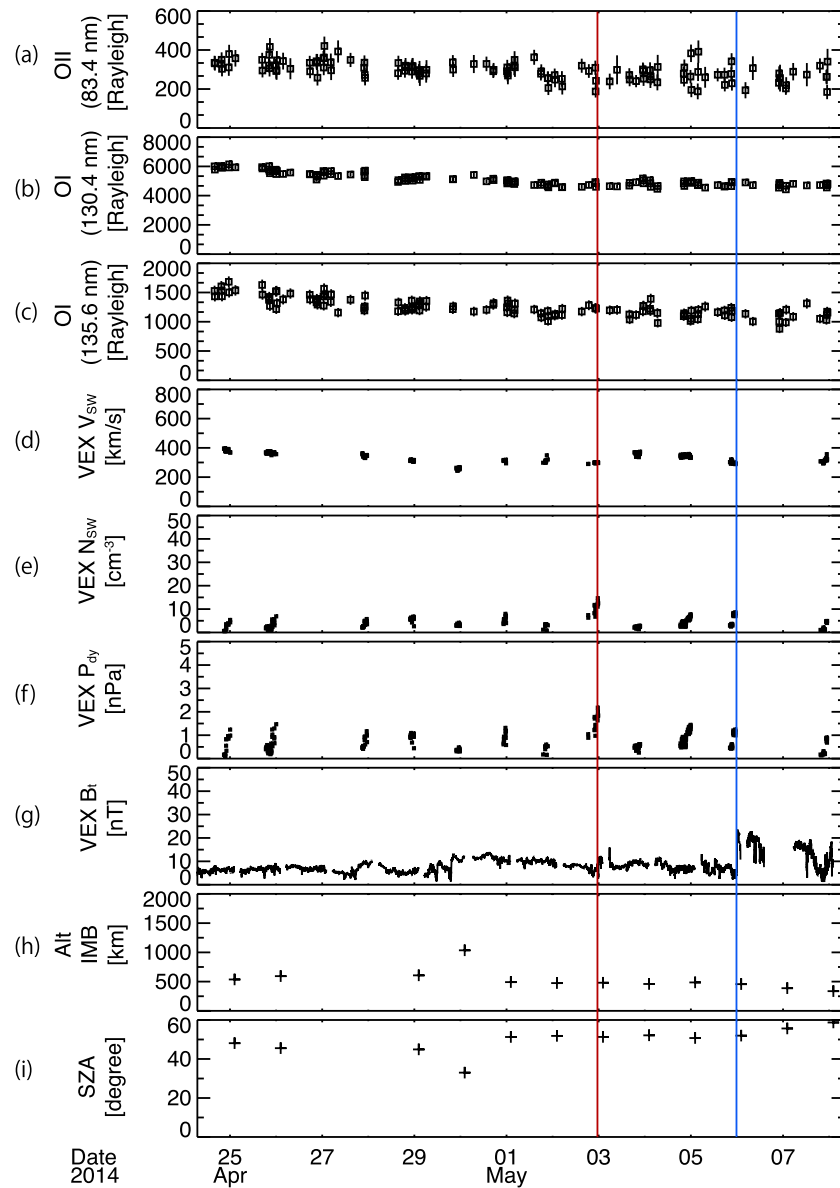


**Figure 8.** Time series of the dayglow brightness, VEX observations of the solar wind and the IMB altitude and the solar zenith angle when VEX crosses the IMB in period 2. The format is the same as Figure 7. The red and blue vertical lines indicate the time when the enhancement of the solar wind dynamic pressure or of the magnetic field is observed, respectively.

Figure 9 shows the time series of the disk brightness and the solar wind magnetic field in period 3. In this period, we only show the magnetic field as the solar wind parameter due to the limited operation of ASPERA-4 in the solar wind for the aerobraking campaign of Venus Express. In this period three enhancements of the magnetic field are seen as shown by blue vertical lines, but we do not see common features in each of the brightness emissions.

Next, we study relations in periodicities between the disk brightness and the solar wind parameters. Figure 10 shows the power spectra of the solar wind parameters plotted over spectra of the disk brightness for OI 135.6 nm. Note that we chose OI 135.6 nm for the comparison because this emission is mostly excited by photoelectron impacts. Note also that we detected similar spectra for the other two emissions in this period. Figures 10a and 10b show power spectra of the solar wind velocity and dynamic pressure (red) with that of the variation for OI 135.6 nm (black) calculated by the LSP method in period 1. As mentioned, two CIRs reached Venus per ~ 10 days, so we see a clear peak at 9.9 day in the solar wind velocity in Figure 10a, which corresponds to the 9.9 day periodicity observed in the brightness of OI 135.6 nm. The other periodicities of the solar wind

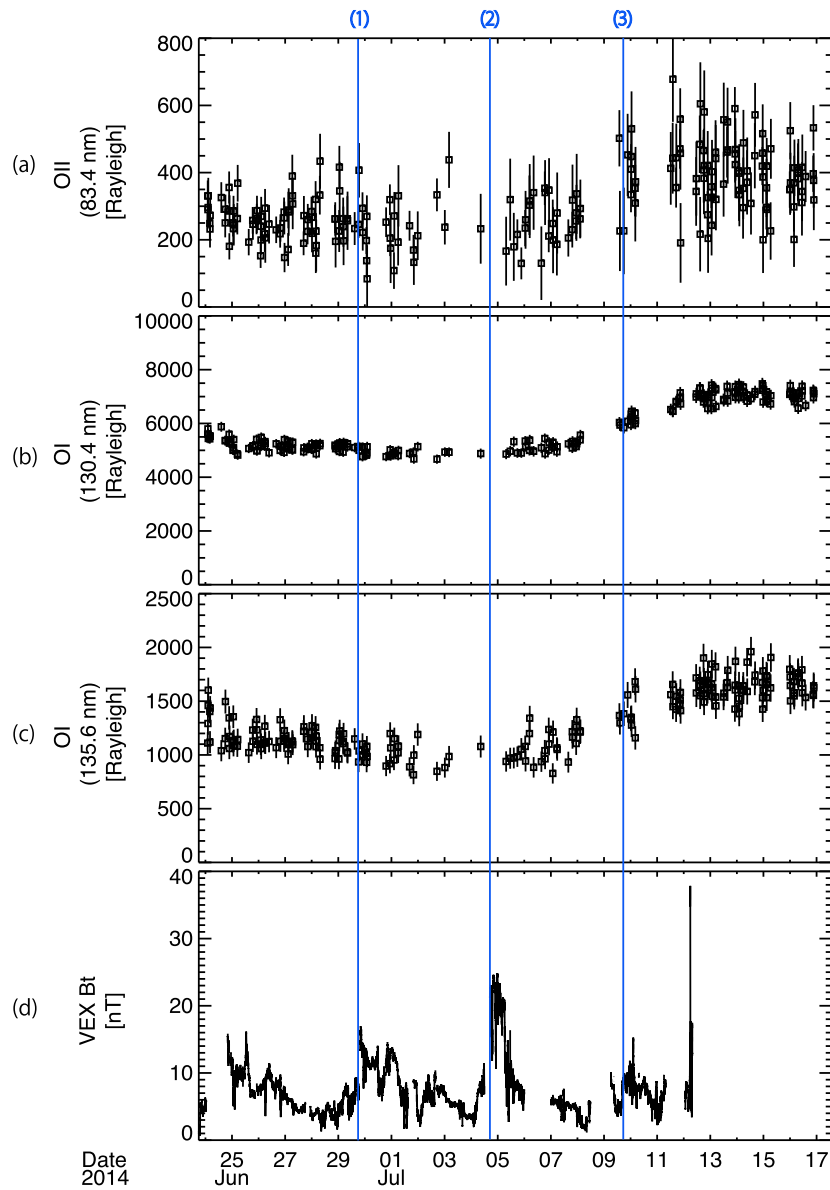


**Figure 9.** Time series of (a–c) the dayglow brightness and (d) the VEX IMF intensity. The blue lines indicate the enhancement of the magnetic field intensity.

velocity do not correspond to the other periodicities of the brightness of OI 135.6 nm (i.e., ~2.8 day and ~4.5 day). As seen in Figure 10b the dynamic pressure in this period has a main peak periodicity of 6.6 days, which does not correspond to any of the dayglow’s periodicities in period 1. The dynamic pressure has the other periodicities as well. One peak at 2.6 day is close to the 2.8 day periodicity seen in the brightness of OI 135.6 nm. Due to the large lack of the magnetic field data, we do not study the effect of the IMF intensity in this period.

Figures 10c–10e show the power spectra of the solar wind velocity (red), dynamic pressure (red), and the IMF intensity (blue) plotted over the OI 135.6 nm spectrum (black) calculated by the LSP method in period 2. As seen in Figure 10c, the spectrum of the solar wind velocity has several periodicities. One of them at ~1.2 day is close to the periodicity of the OI 135.6 nm brightness at ~1.1 day. The solar wind dynamic pressure and the IMF intensity have a peak periodicity at ~2.1 days and ~7.0 days, respectively (see Figures 10d and 10e), which shows that both of these periodicities are different from those of the OI 135.6 nm brightness. One of the minor periodicities of 1.1 day detected both in the dynamic pressure and the IMF intensity corresponds to the one of the periodicities of the OI 135.6 nm brightness.

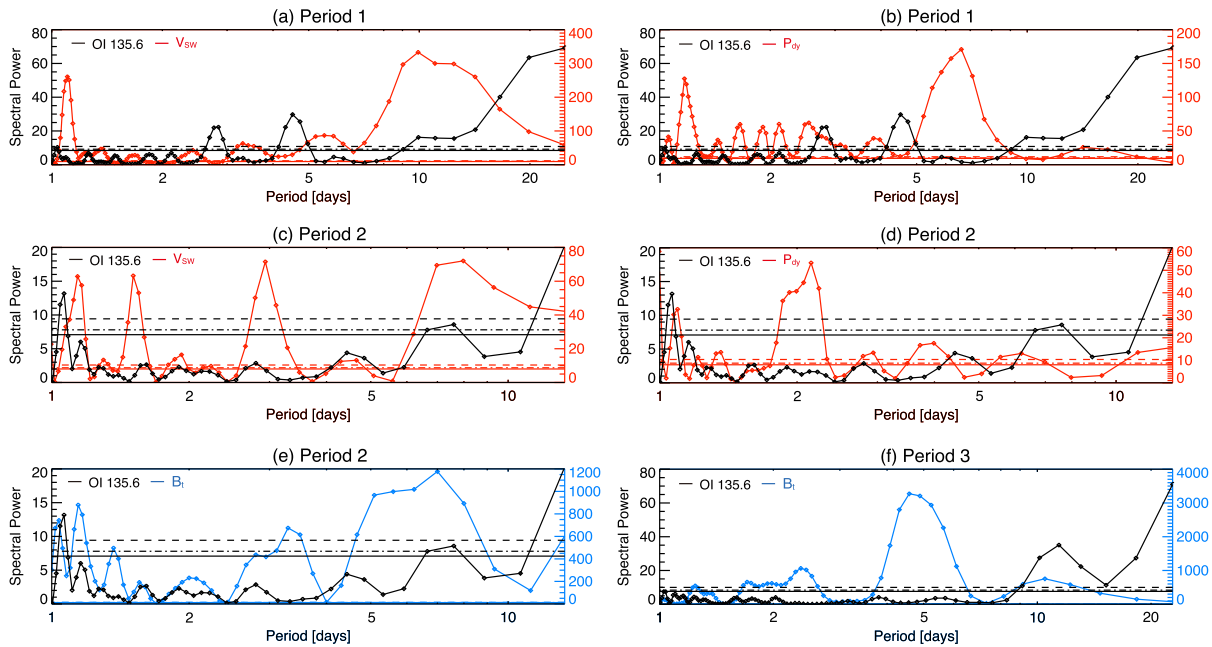


**Figure 10.** Power spectra of the solar wind velocity and the dynamic pressure (red) plotted over that of the dayglow brightness for OI 135.6 nm (black) (a, b) in period 1 and (c, d) in period 2. (e, f) Power spectra of the IMF intensity (blue) plotted over that of the brightness variations for OI 135.6 nm (black) in period 2 and period 3. The 90%, 95% and 99% confidence levels are indicated by the horizontal solid line, the dash-dotted line, and the dashed line, respectively. Note that color of these lines corresponds to the color of each spectrum.

Figure 10f shows a normalized power spectrum of the IMF intensity (blue) and the brightness of OI 135.6 nm (black) derived by using the LSP method. The main peak period of the magnetic field is 4.6 days, which does not correspond to that of the OI 135.6 nm brightness. One of the secondary peaks of the spectrum of the magnetic field is 10 days, which is close to the 11 day periodicity of the brightness of OI 135.6 nm.

#### 4. Discussion

Periodic variations of the EUV oxygen dayglow brightness for OII 83.4 nm, OI 130.4 nm, and OI 135.6 nm are observed in the Venesian thermosphere over the three periods in 2014. Table 1 shows a summary of the periodicities of the disk brightness and relevant periodicities of the solar radiation flux and the solar wind parameters to the disk brightness. The most characteristic variations in the brightness are seen in period 1. In this period, each variation and spectrum look very similar. The 4.5 day periodicity is dominant for all emissions, and secondary periodicities are also detected in the brightness for OI 130.4 nm (~1.8 day, ~2.8 day, and ~3.1 day) and OI 135.6 nm (~2.8 day and ~9.9 day). In periods 2 and 3, the variations of the

**Table 1.** Summary of Characteristic Periodicities in the Oxygen Dayglow Brightness ( $I_{83.4}$ ,  $I_{130.4}$ , and  $I_{135.6}$ ), the Solar EUV Radiation Flux ( $F_{EUV}$ ), and the Solar Wind Parameters ( $V_{SW}$ ,  $P_{dy}$ , and  $B_t$ ) in Each Period<sup>a</sup>

Period	1	2	3
$I_{83.4}$	4.5 day	X	1.0 day and 11 day
$I_{130.4}$	1.8 day, 2.8 day, 3.1 day, and 4.5 day	1.1 day	1.0 day and 11 day
$I_{135.6}$	2.8 day, 4.5 day, and 9.9 day	1.1 day	11 day
$F_{EUV}$	4.3 day and 9.9 day?	X	11 day?
$V_{SW}$	9.9 day	1.2 day	-
$P_{dy}$	2.6 day	1.1 day	-
$B_t$	-	1.1 day	10 day

<sup>a</sup>Note that we do not show all the periodicities observed in the EUV radiation flux and the solar wind parameters but only show periodicities nearly corresponding to the characteristic periodicities in the oxygen dayglow. The dash and the cross indicate no observations and no detections of characteristic periodicities close to the characteristic dayglow periodicities, respectively. The periodicities with a question mark show unclear periodicities because a clear peak is not visible even though the power exceeds the significant level of 99%.

brightness of OI 130.4 nm and OI 135.6 nm look similar although similarity is uncertain for the OII 83.4 nm due to the large variances in the data. In those periods, a periodicity of  $\sim 1.1$  day is detected for OI 130.4 nm and OI 135.6 nm in period 2, and periodicities of  $\sim 11$  day for all emissions and  $\sim 1.0$  day for OII 83.4 nm and OI 130.4 nm are detected in period 3. Over the three periods, the amplitude of the variation for OI 135.6 nm residual brightness is 6.6–10%. This means that O atom densities or photoelectron densities vary several percent above a certain altitude ( $\sim 130$  km) in the Venusian upper atmosphere. Note that OI 130.4 nm emission is optically thick and thus the amplitude of the residual brightness is not proportional to the density modulation. Note also that the 12–27% variations for the OII 83.4 nm are likely to be statistical errors rather than density variations. Since the disk brightness is derived from integrations over the total disk, the physical process controlling the periodic variation would be a global phenomenon or a strong local phenomenon. We suggest that the periodic variations are caused by density modulations of oxygen atoms or photoelectrons in the Venus upper atmosphere.

One possible candidate for the density modulations is planetary-scale waves [Forbes and Konopliv, 2007]. If such waves propagate vertically into the thermosphere and if they break at certain altitudes, density modulations of O atoms would occur globally in the Venus thermosphere. According to previous studies [e.g., Del Genio and Rossow, 1990], typical planetary-scale waves observed at Venus are the Kelvin waves and the Rossby waves. It is shown that periodicities of the Kelvin waves and the Rossby waves are  $\sim 4$  days and 5.6 days, respectively [Del Genio and Rossow, 1990]. These periodicities are roughly consistent with the 4.5 day periodicity we have observed in period 1. The 1.8 day, 2.8 day/3.1 day, 9.9 day, and 11 day periodicities observed over the three periods may be related to the 1.6 day, 2.6–2.9 day, 9.3 day, and 10 day waves mentioned in Forbes and Konopliv [2007]. The 2.6–2.9 day waves are known based on several observations in or above the cloud level [Del Genio and Rossow, 1982; Covey and Shubert, 1982; Apt and Leung, 1982]. The 10 day wave is observed in the dayside thermosphere of Venus [Forbes and Konopliv, 2007]. The 9.3 day and 1.6 day waves could be produced by nonlinear interactions between the 4 day and 2.8 day waves [Forbes and Konopliv, 2007].

Recently, Kouyama et al. [2015] suggested that these waves preferably propagate upward to the cloud top level at 80 km altitude depending on background wind flows. Hoshino et al. [2012] showed that the Kelvin waves and the Rossby waves propagate to the thermosphere from 80 km altitudes on Venus by using their GCM. Combining the result of Hoshino et al. [2012] with that of Kouyama et al. [2015], these waves could propagate to the thermosphere with certain amplitudes. The cause of the change of the main periodicity over the three periods as seen in the three dayglow variations remains unknown, but wind velocities around the cloud top level may play a key role for the vertical propagation of planetary-scale waves [Kouyama et al., 2015]. In theory, however, the planetary-scale waves are strongly affected by the radiative damping under nonzero background flows when they vertically propagate. Thus, it is difficult for the amplitude of the planetary waves to be grown to exceed the background wind speed above the cloud tops. To confirm the scenario, monitoring planetary-scale waves in the middle atmosphere and wind profiles above the cloud tops simultaneously with Hisaki is important.

Another possible candidate for the density modulation is gravity waves generated in the middle atmosphere [Alexander, 1992]. If the gravity waves propagate vertically into the thermosphere and saturate there, local eddy diffusions are enhanced. The enhanced eddy diffusions transport O atoms downward but CO<sub>2</sub> molecules upward, resulting in decreasing the O/CO<sub>2</sub> ratio in the thermosphere. If the wave source lies in the superrotating atmosphere, the eddy diffusions modulate O atom densities with  $\sim 4$  day period in the thermosphere, which roughly corresponds to the  $\sim 4.5$  day periodicity observed in period 1. We suggest that the change of the power of the  $\sim 4.5$  day periodicity over the three periods may come from a local enhancement of eddy diffusions in the dawnside of Venus, resulting in the dawn-dusk asymmetry of O densities in the thermosphere [Alexander et al., 1993]. Since the 4.5 day periodicity is observed only in period 1, when Hisaki points to the morning side of Venus, but not in period 2 and period 3, when Hisaki points to the noonside of Venus, our results may indicate that there are local time differences in wave filtering structures or in wave braking altitudes. However, the gravity wave hypothesis does not provide proper explanations for the  $\sim 1.0$  day,  $\sim 1.1$  day,  $\sim 1.8$  day,  $\sim 2.8$  day,  $\sim 3.1$  day,  $\sim 9.9$  day, and  $\sim 11$  day periodicities. Since the source of the gravity waves, their spatial distribution, and their breaking levels are not known well, more research on the gravity waves on Venus are needed.

The solar wind also could be a possible candidate for the density modulations in the thermosphere [Lei *et al.*, 2008]. By investigating time series of simultaneous measurements of the solar wind velocity, dynamic pressure and the IMF intensity with the residual dayglow brightness, we did not find a clear correlation in the dayglow variations. However, some of the periodicities detected in the solar wind parameters are close to those seen in the residual dayglow brightness (cf. 9.9 day in Figure 10a, 2.8 day in Figure 7b, 1.1 day in Figures 10c–10e, and 10 day in Figure 10f). The cause of the similarities of the periodic modulations is still unknown, but modulations of the photoelectron densities in the ionosphere induced by the solar wind modulations could be a possible scenario. To figure it out, more simultaneous observations of the solar wind with the EUV dayglow are needed. Since Venus Express ended its mission at the end of December 2014, it is important to send a new plasma instrument to Venus to investigate the solar wind's contribution to the Venus upper atmosphere. It is also important to develop accurate solar wind models to compensate absence of in situ plasma measurements at Venus.

Periodic variations of the solar radiation flux could also cause periodic modulations of the photoelectron densities in the Venus ionosphere. Over the three periods, several minor periodicities are detected other than the solar rotational effect (~27 days). In period 1, the solar radiation flux shows the ~4.3 day periodicity which is close to the ~4.5 day periodicity of the dayglow brightness. Additionally, we see significant power around the periodicities where the characteristic dayglow periodicities are detected (~9.9 day in period 1 and ~11 day in period 3) even though a clear peak is not visible. In period 2, however, the minor periodicities of the solar radiation flux do not correspond to the characteristic dayglow periodicity. Thus, it is uncertain to explain the effect of the minor modulations in the solar radiation flux on the periodic dayglow variations. We need longer-term and more continuous observations to confirm this effect.

There are still many open questions to understand the periodic variations of the oxygen dayglow in the upper atmosphere of Venus. In the near future Hisaki will observe Venus again. Looking at the EUV dayglow in the duskside of Venus may give us new characteristic features and new insights for these questions.

## 5. Conclusion

We observed EUV oxygen dayglow for OII 83.4 nm, OI 130.4 nm, and OI 135.6 nm at Venus observed by EXCEED aboard Hisaki in three quasi-continuous periods in 2014: March–April (period 1), April–May (period 2), and June–July (period 3). The dayglow brightness of the three emissions mainly varies with the solar EUV radiation flux since it controls the amount of photoelectrons in the Venus ionosphere. We also find characteristic periodicities in each period. In period 1, 4.5 day periodicity is observed in the brightness for the three emissions. Secondary periodicities at 1.8 day, 2.8 day, and 9.9 day are also detected in period 1. 1.1 day periodicity is detected in period 2, and 1.0 day and 11 day periodicities are detected in period 3. The amplitude of the variation is 6.6–10% for OI 135.6 nm, which means that O atom densities or photoelectron densities globally vary by several percent in the thermosphere above ~130 km. We suggest that the periodic variations are a result of density modulations of oxygen atoms or photoelectrons in the Venusian thermosphere. The cause of the periodic variations is still uncertain, but planetary-scale waves and/or the gravity waves propagating from the middle atmosphere of Venus, and/or minor periodic variations of the solar EUV radiation flux may play a role. Effects of the solar wind on the dayglow variations are also investigated by using the solar wind measurements of ASPERA-4 and MAG aboard VEX, but a clear correlation with the dayglow variations is not found. However, minor periodicities detected in the solar wind velocity, the dynamic pressure, and the interplanetary magnetic field's intensity are close to those of the dayglow brightness. The contribution of these parameters to the dayglow remains still unknown, but they may affect the dayglow periodic variations. What controls the periodic variations of the EUV dayglow at Venus is still an open question. For future study, it is important to observe wave activities and wind profiles in the middle atmosphere of Venus by ground-based observatories simultaneously with Hisaki observations to extend understandings of the connection between the middle atmosphere and the upper atmosphere of Venus.

## References

- Alexander, M. J. (1992), A mechanism for the Venus thermospheric superrotation, *Geophys. Res. Lett.*, *19*(22), 2207–2210, doi:10.1029/92GL02110.
- Alexander, M. J., A. I. F. Stewart, S. C. Solomon, and S. W. Boucher (1993), Local time asymmetries in the Venus thermosphere, *J. Geophys. Res.*, *98*(E6), 10,849–10,871, doi:10.1029/93JE00538.
- Apt, J., and J. Leung (1982), Thermal periodicities in the Venus atmosphere, *Icarus*, *49*, 427.

### Acknowledgments

This work was supported by Grant-in-Aid for JSPS Fellows 14J03613 from Japan Society for the Promotion of Science (JSPS). This work was partially supported by Grant-in-Aid for Scientific Research (B) 15H03731 as well as by the Program for Advancing Strategic International Networks to Accelerate the Circulation of Talented Researchers G2602 from JSPS and MEXT of Japan. We are grateful to Takeshi Imamura for giving us helpful comments on this paper. We would like to thank all the Hisaki project members for the effort leading to the successful mission. We also would like to thank the SOHO/SEM team, the VEX/ASPERA-4 team, and the VEX/MAG team for developing the instruments and for making us possible to access data. The Hisaki/EXCEED data is archived in the Data Archives and Transmission System (DARTS), JAXA (<https://hisaki.darts.isas.jaxa.jp/>). The SOHO/SEM data can be downloaded at [http://www.usc.edu/dept/space\\_science/sem\\_data/downloadSEM.html](http://www.usc.edu/dept/space_science/sem_data/downloadSEM.html). The VEX data are available at <http://amda.cdpp.eu/>.

- Barabash, S., et al. (2007), The Analyser of Space Plasma and Energetic Atoms (ASPERA-4) for the Venus Express mission, *Planet. Space Sci.*, *55*, 1772–1792.
- Bertaux, J. L., J. Blamont, V. M. Lepine, V. G. Kurt, N. N. Romanova, and A. S. Smirnov (1981), Venera 11 and Venera 12 observations of EUV emissions from the upper atmosphere of Venus, *Planet. Space Sci.*, *29*, 149–166.
- Bougher, S. W., M. J. Alexander, and H. G. Mayr (1997), *Upper Atmosphere Dynamics: Global Circulation and Gravity Waves, Venus II*, chap. 2.4, pp. 259–292, Univ. Ariz. Press, Tucson.
- Broadfoot, A. L., S. Kumar, M. J. Belton, and M. B. McElroy (1974), Ultraviolet observations of Venus from Mariner 10: Preliminary results, *Science*, *183*, 1315–1318.
- Coates, A. J., et al. (2008), Ionospheric photoelectrons at Venus: Initial observations by ASPERA-4 ELS, *Planet. Space Sci.*, *56*, 802–806.
- Covey, C., and G. Shubert (1982), Planetary-scale waves in the Venus atmosphere, *J. Atmos. Sci.*, *39*, 2397–2413.
- Del Genio, A. D., and W. B. Rossow (1982), Temporal variability of ultraviolet cloud features in the Venus stratosphere, *Icarus*, *51*, 391–415.
- Del Genio, A. D., and W. B. Rossow (1990), Planetary-scale waves and the cyclic nature of cloud top dynamics on Venus, *J. Atmos. Sci.*, *47*(3), 293–318.
- Domingo, V., B. Fleck, and A. I. Poland (1995), The SOHO mission: An overview, *Sol. Phys.*, *162*, 1–37.
- Feldman, P. D., E. B. Burgh, S. T. Durrance, and A. F. Davidsen (2000), Far-ultraviolet spectroscopy of Venus and Mars at 4 angstrom resolution with the Hopkins Ultraviolet Telescope on ASTRO-2, *Astrophys. J.*, *538*, 395–400.
- Forbes, J. M., and A. Konopliv (2007), Oscillation of Venus' upper atmosphere, *Geophys. Res. Lett.*, *34*, L08202, doi:10.1029/2007GL029252.
- Gérard, J.-C., B. Hubert, J. Gustin, V. I. Shematovich, D. Bisikalo, G. R. Gladstone, and L. W. Esposito (2011), EUV spectroscopy of the Venus dayglow with UVIS on Cassini, *Icarus*, *211*, 70–80.
- Hord, C. W., et al. (1991), Galileo ultraviolet spectrometer experiment: Initial Venus and interplanetary cruise results, *Science*, *253*, 1548–1550.
- Hoshino, N., H. Fujiwara, M. Takagi, Y. Takahashi, and Y. Kasaba (2012), Characteristics of planetary-scale waves simulated by a new venusian mesosphere and thermosphere general circulation model, *Icarus*, *217*, 818–830.
- Hovestadt, D., et al. (1995), CELIAS—Charge, element and isotope analysis system for SOHO, *Sol. Phys.*, *162*, 441–481.
- Hubert, B., J. C. Gérard, J. Gustin, V. I. Shematovich, D. V. Bisikalo, A. I. Stewart, and G. R. Gladstone (2010), UVIS observations of the FUV OI and CO 4P Venus dayglow during the Cassini flyby, *Icarus*, *207*, 549–557.
- Kouyama, T., T. Imamura, M. Nakamura, T. Satoh, and Y. Futaana (2015), Vertical propagation of planetary-scale waves in variable background winds in the upper cloud region of Venus, *Icarus*, *248*, 560–568.
- Lei, J., J. P. Thayer, J. M. Forbes, E. K. Sutton, and R. S. Nerem (2008), Rotating solar coronal holes and periodic modulation of the upper atmosphere, *Geophys. Res. Lett.*, *35*, L10109, doi:10.1029/2008GL033875.
- Lellouch, E., T. Clancy, D. Crisp, A. Kliore, D. Titov, and S. W. Bougher (1997), *Monitoring of Mesospheric Structure and Dynamics, Venus II*, chap. 3.1, pp. 295–324, Univ. Ariz. Press, Tucson.
- Lomb, N. R. (1976), Least-squares frequency analysis of unequally spaced data, *Astrophys. Space Sci.*, *39*, 447–462.
- Moos, H. W., and G. J. Rottman (1971), O I and H I emissions from the upper atmosphere of Venus, *Astrophys. J.*, *169*, L127–L130.
- Nakagawa, H., N. Hoshino, M. Sornig, Y. Kasaba, G. Sonnabend, D. Stupar, S. Aoki, and I. Murata (2013), Comparison of general circulation model atmospheric wave simulations with wind observations of venusian mesosphere, *Icarus*, *225*, 840–849.
- Phillips, J. L., J. G. Luhmann, and C. T. Russell (1985), Dependence of Venus ionopause altitude and ionospheric magnetic field on solar wind dynamic pressure, *Adv. Space Res.*, *5*(9), 173–176.
- Russell, C. T., and O. L. Vaisberg (1983), *The Interaction of the Solar Wind With Venus*, pp. 873–940, Univ. Ariz. Press, Tucson, AZ.
- Scargle, J. D. (1982), Studies in astronomical time series analysis. II—Statistical aspects of spectral analysis of unevenly spaced data, *Astrophys. J.*, *263*, 835–853.
- Spenner, K., Z. Dóbe, A. F. Nagy, W. C. Knudsen, and W. Lotze (1997), Photoelectron fluxes in the Venus dayside ionosphere, *J. Geophys. Res.*, *102*(A2), 2577–2583, doi:10.1029/96JA03341.
- Stewart, A. I., D. E. Anderson Jr., L. W. Esposito, and C. A. Barth (1979), Ultraviolet spectroscopy of Venus: Initial results from the pioneer Venus orbiter, *Science*, *203*, 777–779.
- Takagi, M., and Y. Matsuda (2007), Effects of thermal tides on the Venus atmospheric superrotation, *J. Geophys. Res.*, *112*, D09112, doi:10.1029/2006JD007901.
- Yamamoto, M., and H. Tanaka (1997), Formation and maintenance of the 4-day circulation in the Venus middle atmosphere, *J. Atmos. Sci.*, *54*, 1472–1489.
- Yamazaki, A., et al. (2014), Field-of-view guiding camera on the Hisaki (SPRINT-A) satellite, *Space Sci. Rev.*, *184*, 259–274.
- Yoshikawa, I., et al. (2014), Extreme ultraviolet radiation measurement for planetary atmospheres/magnetospheres from the Earth-orbiting spacecraft (Extreme Ultraviolet Spectroscopy for Exospheric Dynamics: EXCEED), *Space Sci. Rev.*, *184*, 237–258.
- Yoshioka, K., G. Murakami, A. Yamazaki, F. Tsuchiya, M. Kagitani, T. Sakanoi, T. Kimura, K. Uemizu, K. Uji, and I. Yoshikawa (2013), The extreme ultraviolet spectroscopy for planetary science, EXCEED, *Planet. Space Sci.*, *85*, 250–260.
- Zhang, T. L., J. G. Luhmann, and C. T. Russell (1991), The magnetic barrier at Venus, *J. Geophys. Res.*, *96*(A7), 11,145–11,153, doi:10.1029/91JA00088.
- Zhang, T. L., et al. (2006), Magnetic field investigation of the Venus plasma environment: Expected new results from Venus Express, *Planet. Space Sci.*, *54*, 1336–1343.